Macro-Mixing characterisation of a stirred model fermenter of non-NEWTONIAN liquid by flow following sensor particles and ERT

Reinecke, S.; Deutschmann, A.; Jobst, K.; Hampel, U.;

Originally published:

December 2016

Chemical Engineering Research and Design 118(2017), 1-11

DOI: https://doi.org/10.1016/j.cherd.2016.12.002

Perma-Link to Publication Repository of HZDR:

https://www.hzdr.de/publications/Publ-22185

Macro-Mixing characterisation of a stirred model fermenter of non-Newtonian liquid by flow following sensor particles and ERT

Sebastian Felix Reinecke[1,*], Anne Deutschmann[2], Karin Jobst[2], Uwe Hampel[1,3]

[1]Institute of Fluid Dynamics, Helmholtz-Zentrum Dresden-Rossendorf e.V., Germany

[2]Department of Environmental Engineering and Bioenergy, Fraunhofer Institute for Ceramic Technologies and Systems (Fraunhofer IKTS), Dresden, Germany

[3]AREVA Endowed Chair of Imaging Techniques in Energy and Process Engineering, Technische Universität Dresden, Germany

[*]Sebastian Felix Reinecke (s.reinecke@hzdr.de)

ABSTRACT

Investigation of the fluid circulation and the macro-mixing process in a stirred model fermenter of non-Newtonian liquid was conducted by the comparative use of flow following sensor particles, ERT and CFD. Average fluid circulation times were estimated from (i) the measured vertical position of the sensor particle, (ii) the fluctuating ERT signals of single ERT planes and (iii) the simulated dispersed phase. The estimated average circulation times of all the three methods are comparable for the two investigated impeller positions. Furthermore, axial residence profiles of the sensor particles were extracted, which reveal the impact of the impeller configuration to the axial mixing homogeneity. Moreover, the results confirm the conclusions about the effect of the off-bottom clearance of the impeller derived by Reinecke et al. (2012) in a 1000 L pilot fermenter. The excellent detectability of the particles and the consistent results confirm the feasibility of the combined method for further investigation of the complex flows in biogas fermenters.

Keywords macro mixing, circulation time, hydrodynamics, stirred tank, biogas fermenter, flow follower, sensor particle, ERT, CFD

Highlights

- The fluid circulation flow in a stirred model fermenter of non-Newtonian liquid is investigated.
- In this study results of flow following sensor particles are compared to ERT and CFD data.
- Mixing homogeneity is evaluated by the axial residence profiles of the sensor particle.
- Fluid circulation times estimated by sensor particles are confirmed by ERT and CFD.

1 INTRODUCTION

Investigation and further optimization of chemical and power engineering processes require advanced monitoring techniques. Especially the acquisition of the spatio-temporal distribution of process parameters in large-scale vessels such as stirred chemical or bioreactors is of great interest. Beyond investigation of biochemical parameters, such as the fermentation rate, pH distribution and oxygen reduction potential, also knowledge of hydrodynamic parameters, such as flow velocity profiles, circulation times, energy dissipation, suspension mixing (homogeneity, location of dead zones and short-circuits) and heat transfer (temperature profiles), it is necessary to evaluate the efficiency of e.g. heating and mixing regimes. However, in most industrial scale applications, where sensor mounting or

cable connections are not feasible or desired, the acquisition of these parameters and their spatial distributions is hampered by the limited access to the process itself. This applies especially for large-scale biogas fermentation reactors, where state of the art instrumentation is commonly limited to few spatial positions and it is doubtfully assumed that the measured parameters are representative for the whole vessel. Moreover, the size of industrial reactor vessels and the opacity of the fluids and vessel walls does in most cases not allow application of single point flow measurement techniques (LDV and UDV) as well as spatially resolving measurement techniques (videometry, thermography, PIV, LIF and tomography techniques) that are normally used in laboratory and pilot-scale applications (Mavros 2001). A promising technique that has been used in larger vessels up to 20 m^3 is movement tracking of discrete macroscopic particles or flow followers. The technique utilizes a distinct property of the flow follower such as color (video tracking) (Barrue et al. 1999), emitted radio-frequency (Bryant 1969, Day 1975, Barneveld et al. 1987), magnetic permeability (Patterson et al. 2010) or radioactivity (CARPT, PEPT) (Luo et al. 2008, Fangary et al. 2000) to detect the particle and extract the flow properties from the particle trace. However, tracking devices such as aerials, magnetic detectors and radioactivity detectors require traversing to capture the whole reactor volume. This is often impractical in industrial applications, due to heavy constructions and large dimensions of the vessels.

Considering autonomous sensor technologies and remote sensing makes the metrological acquisition of spatially distributed parameters accessible also for industrial applications. Advanced sensors and the increasing capability of highly integrated circuits have enabled the design of intelligent instrumented flow followers with data acquisition, data storage and communication capabilities combined in a small-scale system design. Examples of highly advanced approaches for industrial applications and harsh environments are an ad-hoc sensor network for monitoring of nuclear storage ponds (York et al. 2012) and an acoustic tracking system for instrumented flow followers in confined spaces (Burnett-Thompson and York 2007, Pottinger and York 2011). Further tracking concepts based on sensor systems without embedded communication are the so called ‘Smart’ sphere (Wadke et al. 2005) and a sensor fish (Deng et al. 2007). These achievements approve the feasibility of autonomous sensor technologies for investigation of industrial applications. Nevertheless, further efforts have to be made to enable the acquisition of spatially distributed parameters in the fluid flows of large-scale industrial processes and the evaluation of the hydrodynamics of the process from the measured data.

The concept of self-powered and neutrally buoyant sensor particles has been developed for the long-term measurement of spatially distributed process parameters in the chemically and mechanically harsh environments of agitated industrial vessels (Thiele et al. 2010). One intended application target is flow measurement in stirred fermentation biogas reactors, but generally the sensor particle is not limited to this type of process. A set of sensor particles has already been tested in real flow conditions of a highly viscous bio-substrate in a stirred 1000 L pilot fermenter vessel. The results show that the sensor particles reflect the flow conditions in the vessel qualitatively and that macro-mixing of the process, such as particle circulation times, can be evaluated from the measured sensor particle data sets (Reinecke et al. 2012).

In fact, validation of the sensor particle data from experiments in relevant tank geometries and realistic non-Newtonian fluids is hampered by the limited availability of feasible spatially resolved reference measurement techniques. The well established measurement techniques, such as hard-field and soft-field tomography, videometry and particle image velocimetry, are either not applicable to large-scale vessels or may not be feasible for measurement in the opaque liquors. Montante and Paglianti (2015) investigated the fluid dynamics of a model digester as scale-down of a typical stirred biogas tank design with optically clear liquids by the use of particle image velocimetry. However, this method cannot be applied for real substrates and model fluids with organic fibres.

In this paper we present the results of mixing experiments in a down-scaled stirred vessel (volume 80 L) with a model substrate (2.5 g/L Xanthan solution; ρ = 1004 $kg \cdot m^{-3}$) under comparable conditions as in a pilot fermentation vessel (volume 1000 L). An electrical resistance tomography system (ERT) was applied for the investigation of the mixing process, such as by Mann et al. (1999) and Rodgers et al. (2009). Moreover, also validation of the sensor particles was possible with the ERT, which is a very similar approach as the monitoring of passive flow followers described by Salem et al. (2001). Measurement of two electrode planes (top and bottom plane) was sufficient to investigate integral mixing times from NaCl tracer experiments and to analyse the movement of single sensor particles in the stirred vessel. Two experiments where conducted at a constant impeller speed of n = 4.7 s^{-1} where only the off-bottom clearance of the impeller was changed from 0.086 m to 0.14 m. Comparison of the circulation time was done since it is a valuable macro-mixing parameter.

2 MATERIALS AND METHODS

2.1 Principle of the sensor particle

The sensor particle concept is based on a first prototype (Thiele et al. 2010). Each sensor particle comprises a battery, miniaturized sensors, on-board measurement electronics and a protective capsule. The current setup was fitted to typical biogas fermenter conditions and allows acquisition of the basic physical process parameters, namely temperature (10 °C to 70 °C; u_T = ±0.25 K), immersion depth (u_z = ±2.2·10^{-2} m) as a function of absolute pressure (98 kPa to 158 kPa; u_p = ±229 Pa) and 3D particle acceleration (-2g to +2g; ±0.5mg) (Reinecke 2014). This allows evaluation of local flow (mixing) and fermentation conditions. It is intended to complete the concept by other sensors, such as for position (magnetic field, rotational rate) and chemical parameters (pH/ORP, conductivity). The electronics acquires the signals of the incorporated sensors in an energy efficient measurement scheme. Up to 299,590 full data sets of all sensors can be saved on the on-board data storage. Therefore an approximate runtime of 208 days or 3.3 hours can be covered at acquisition rate 1 min^{-1} or 25 s^{-1}, respectively. The whole electronics is enclosed in a robust neutrally buoyant capsule (equivalent diameter 58 mm), to allow free movement with the flow (Figure 1a).
The sensor particles are applied to a fermentation reactor in following procedure (Figure 1b). After insertion of the sensor particles to the vessel, the particles are dispersed with the substrates. The particles follow the predominant flows in the vessel freely due to their neutrally buoyant character, and acquire the temporal evolution of the selected process parameters. Data are downloaded and analyzed after recovering the particles from the process. After inspection, the sensor particles can be reused. Following this procedure, Reinecke et al. (2012) applied seven sensor particles for a period of 110 min to the pilot fermenter with a volume of 1000 L. The measured data of the individual sensor particles were redundant. This proved the reproducibility of the extracted parameters from different sensor particles and even one applied sensor particle would have given representative results after a measurement period of 110 min. Therefore, a single sensor particle that was set up to reach similar flow conditions of the pilot fermenter experiments was applied to the down-scaled vessel to capture the process conditions for 30 minutes for each impeller position (C_1 and C_2).

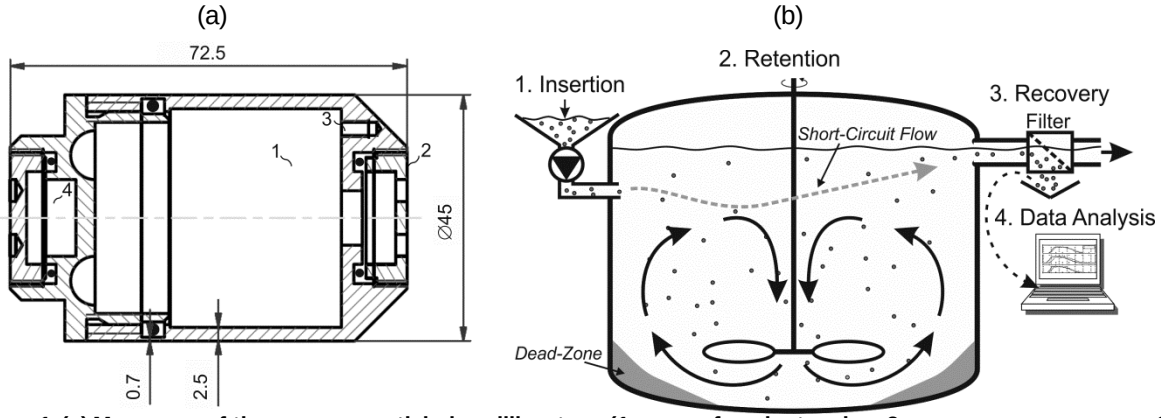

Figure 1. (a) Measures of the sensor particle in millimetres (1: space for electronics; 2: pressure sensor cap; 3: temperature sensor slot; 4: space for payload) and (b) principle of application at an industrial scale reactor.

2.2 Experimental setup of ERT and stirred vessel

The mixing vessel is a model of a pilot fermentation reactor (volume 1000 L) with similar geometry (Figure 2). It has a typical flat geometry of agricultural biogas digesters with a flat bottom and the dimensions T = 0.4 m and H = 0.243 m, where small impellers are applied close to the vessel bottom. The central mixing unit is provided with a 3-bladed PBT impeller with diameter D = 0.14 m, inclination 30° and constant speed N = 4.7 s^{-1}, to simulate similar flow conditions as in the pilot fermenter experiments. Two batch experiments where conducted where only the off-bottom clearance of the impeller was changed from C_1 = 0.086 m to C_2 = 0.14 m. The impeller power number

$$N_P = \frac{P}{\rho \cdot N^3 \cdot D^5} \quad (1)$$

was experimentally estimated by measuring the power consumption P in a Newtonian glycerol with fluid density ρ = 1260 kg·m^{-3} and viscosity μ = 1.395 Pa·s. The power number is shown in Figure 3 in dependence of the impeller Reynolds number

$$\mathrm{Re} = \frac{N \cdot \rho \cdot D^2}{\mu}. \qquad (2)$$

A deviation was not observed between C_1 and C_2. The power number decreases with Reynolds number in the laminar region until it slowly approaches a constant value of 1.0 at higher Reynolds numbers, i.e. in the turbulent region.

The vessel is equipped with an electrical resistance tomography system (ERT; company ITS Plc.; type p2+) (Figure 2) and five tomography planes (plane P1…P5), where each plane has 16 equally spaced stainless steel electrodes. A set of 104 individual voltage measurements is performed for each plane. The conductivity distribution for each plane is then calculated utilising a linear back projection image reconstruction algorithm (ITS system 2000 software). Based on the pixel conductivities also the global average conductivity signal that represents the whole vessel volume was estimated by the ERT data analysis software (ITS system 2000 software). This allows investigation of mixing times and observation of the sensor particle movement in the stirred vessel. An accuracy of ±3% is given by ITS Plc. for the conductivity measurement. The in plane spatial resolution of the ERT system is 5% of the vessel diameter and thus $3.2 \cdot 10^{-2}$ m, as specified by the manufacturer ITS Plc. The vertical spatial accuracy for the measurement of all five planes is assumed to be in the order of the plane distance, namely $\pm 2.5 \cdot 10^{-2}$ m.

The test liquid was an aqueous solution of Xanthan (2.5 g/L; ρ = 1004 kg·m^{-3}) with non-Newtonian rheological behaviour. The latter is described by the Ostwald-de Waele model for the viscosity

$$\mu = K \cdot \dot{\gamma}^{(n-1)} \qquad (3)$$

with consistency index K = 1.269 Pa·s^n and the flow behaviour index n = 0.273 valid up to a shear rate $\dot{\gamma}$ of 20 s^{-1}. The effective Reynolds number in the impeller region (0.78 dm^3) is approximately 448 and is calculated by (2) with the average viscosity $\langle\mu\rangle$ of 0.2046 Pa·s which is derived from the numerical simulations results (see 2.3). The average viscosity in the whole vessel is $\langle\mu\rangle$ = 0.706 Pa·s, that means, the average Reynolds number in the vessel is 130. Therefore, the flow regime in the vessel is in the beginning turbulent regime.

Furthermore, a salt solution of NaCl was added to the liquid to get an appropriate conductivity level of 15 mS/cm for the ERT measurement. During the mixing time measurement, a NaCl tracer volume of 200 mL (211 mS/cm) was added to the liquid level at the centre of the vessel. Measurement of only the two electrode planes P1 and P5 was sufficient to estimate the global average conductivity signal. Therefore an appropriate acquisition rate of 18.4 fps was achieved to capture the voltage values at P1 and P5 for more than 90 seconds by the DAS during the mixing time experiments.

The influence of the relatively large sensor particle volume on the tracing behavior in the circulation flow is estimated from the given experimental conditions based on the particle's Stokes-number according to Reinecke et al. (2012). It is distinguished between the meso-scale in the impeller region and the macro-scale in the circulation flow. The condition to reach equilibrium flow conditions with discrete particles is a maximum Stokes-number of 0.1 which is described by Fangary et al. (2000). The Stokes-number for the circulation flow is calculated based on the circulation time. Assuming a circulation time of more than 3 seconds the Stokes-number is below 0.06 in the fermenter experiment. This estimate of the Stokes-number is only slightly above the one for the larger pilot fermenter with 0.05 due to the high viscosity of the liquid (Reinecke et al., 2012). Nevertheless, the scaling of the model fermenter is not optimal compared to the size of the sensor particle and distortions of the distort the velocity profile in the small vessel geometry may still occur.

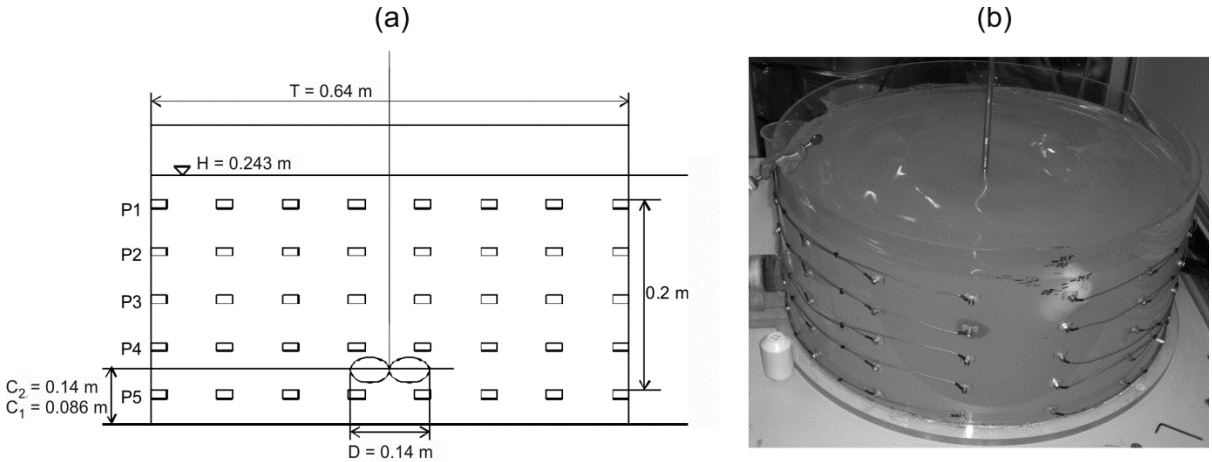

Figure 2. (a) Sketch of the ERT set-up and (b) photograph of the stirred vessel with the floated sensor particle.

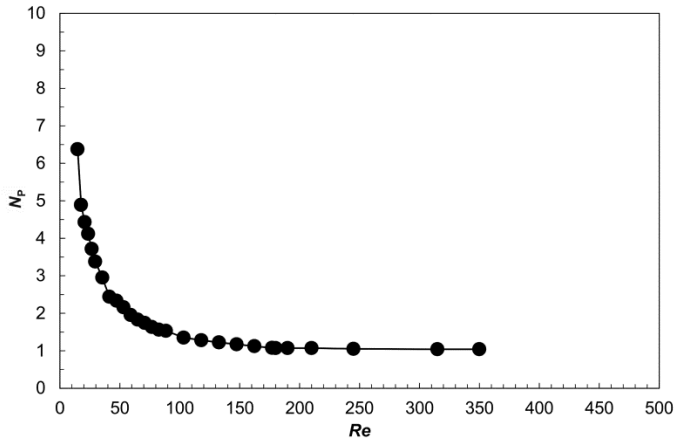

Figure 3. Experimental data of impeller power number *N*p versus Reynolds number Re in a Newtonian glycerol solution.

2.3 Numerical simulation of the stirred vessel

Simulation of dispersed particles in non-Newtonian fluids is limited and the behaviour of the particles cannot be predicted sufficiently (Paschedag, 2004 and Wollny, 2010). The influence of turbulences cannot be described accurately by phase interaction with the Euler/Euler approach, whereas the Euler/Langrange approach shows increased deviations for larger particles compared to the size of the the simulated control volumina. Nevertheless, in order to visualize the flow pattern in the fermenter and to give a first estimate of the circulation time it was simulated using the commercial software package ANSYS CFX 14.0. The multiple frames of reference method is applied to model the agitated impeller. A mesh of 24604 elements for the static region of the fermenter and 12440 elements for the moving impeller region was generated using the ANSYS CFX-mesh tool with the method of Euler/Euler. Turbulences are modelled fluid dependent. Comparison of several turbulence models by Wu (2011) and Zhang et al. (2016) for low Reynolds number turbulent regimes in anaerobic digesters showed acceptable results for the standard k-ε model. However, the predictions of the simulations were still acceptable. Since the flow regime is considered to be in the beginning turbulent regime, the k-ε turbulence model was used for the fluid phase. The dispersed phase was considered as a dispersed fluid with the zero equation model. The drag force was calculated with the Schiller-Naumann condition. The continuous non-Newtonian liquid is set to the properties of the aqueous solution of Xanthan (2.5 g/L; ρ = 1004 kg·m^{-3}) as in the experiment. Also, a dispersed phase with the same density as the liquid, a particle diameter of 58 mm and a concentration of 0.001, i.e. a single particle, is introduced to simulate the behaviour of the sensor particle used in the experiment. The accuracy of the simulated result is estimated to be in the range of ±8% according to the comparable simulation

conditions analysed by Bruening (2012). Based on the vessel dimensions the accuracy of the CFD results is estimated to $u_{z,CFD} = 2 \cdot 10^{-2}$ m in vertical and $u_{h,CFD} = 5 \cdot 10^{-2}$ m in horizontal direction.

3 RESULTS AND DISCUSSION

3.1 Simulated Flow Pattern and Streamlines

The simulated flow pattern of the liquid and the dispersed phase are shown for C_1 and C_2 in Figure 4 and 4. The liquid circulation flow is clearly visible. It is obvious that the fluid velocity is very low in the far region of the impeller due to the high viscosity of the shear-thinning liquid. For C_2 a wider region of the fluid is mobilized with a slightly higher velocity before and after passing the impeller compared to C_1. In general, the flow pattern of the liquid phase and the dispersed particle are almost identical.

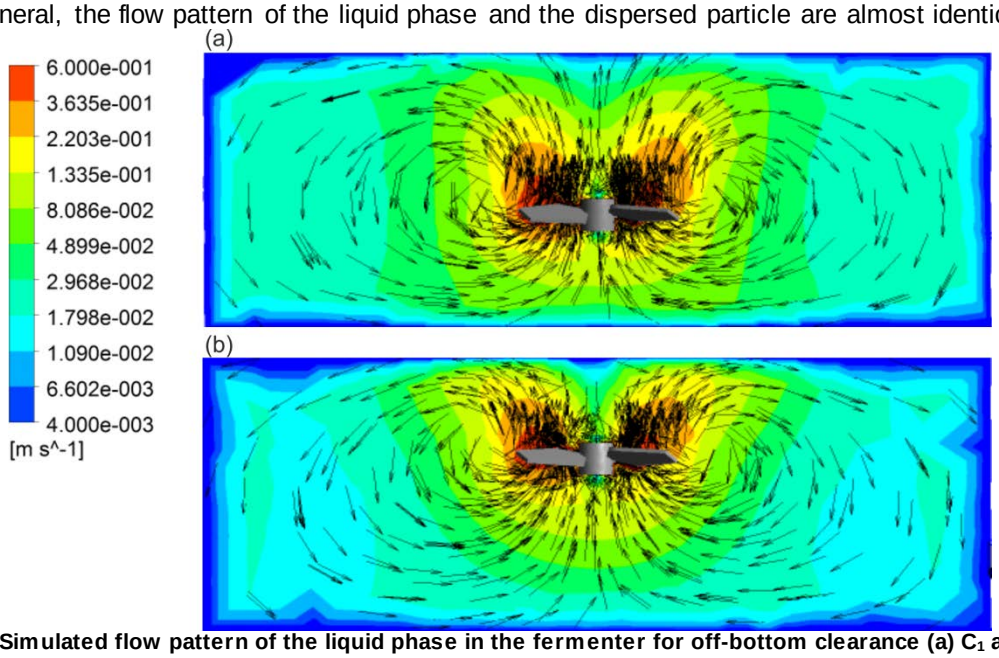

Figure 4. Simulated flow pattern of the liquid phase in the fermenter for off-bottom clearance (a) C_1 and (b) C_2.

Also the streamlines for the liquid and the dispersed phase show a comparable pattern (Figure 5). The pattern is different for C_1 and C_2 which is visible from the streamlines for the liquid and the dispersed phase comparably. In conclusion, the simulated dispersed phase indicates an adequate flow tracing ability of the sensor particles in the fermenter. This is also in agreement with the experimental study of the flow following character of sensor particles (Reinecke, 2014).

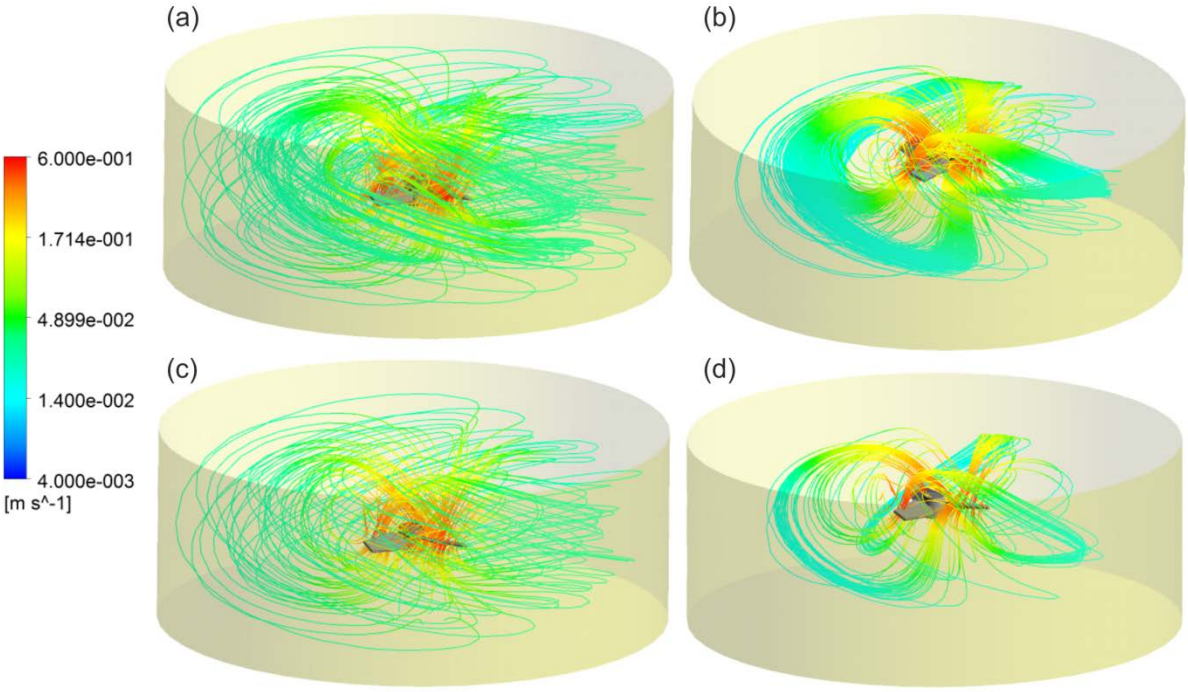

Figure 5. Velocity on streamlines from the simulation of the fermenter for off-bottom clearance (a,c) C_1 and (b,d) C_2 and for (a,b) the liquid phase and (c,d) the dispersed phase.

An estimate of the circulation time for comparison with the measurements of ERT and sensor particle is derived from the streamlines of the dispersed phase. According to the ERT method, the streamlines of the dispersed phase were analysed regarding the passage of the reference plane equivalent to ERT plane P1. A number of 23 passages were detected for C_1 in a period of 90 s which makes an average circulation time of 3.9 s and for C_2 a number of 24 passages were detected in a period of 100 s which makes an average circulation time of 4.2 s.
A first estimate of the uncertainty $u_{tc,CFD}$ of the circulation time is derived by the propagation of the given accuracy $u_{z,CFD}$ of the simulation in vertical direction with the average vertical velocity of the simulated particle on the streamline at the reference plane by

$$u_{tc,CFD} = \frac{u_{z,CFD}}{v_z}. \quad (4)$$

The average vertical velocity of the simulated particle at the reference plane is 0.03 $m \cdot s^{-1}$ for C_1 and 0.02 $m \cdot s^{-1}$ for C_2. Thus, according to (4) $u_{tc,CFD}$ is 0.7 s and 1.0 s for C_1 and C_2, respectively. This uncertainty implies an acceptable deviation of 18% and 24%, respectively. This meets the findings of the CFD study of turbulence models for non-Newtonian flow by Wu (2011) where the errors are estimated within 30% and still reliable predictions which are in reasonable agreement with the measurements are achieved also by the standard k-ε-model.

3.2 ERT Results

3.2.1 Fluid mixing times and characteristic circulation times

Detection of integral mixing times was performed measuring only the top and bottom planes (P1 and P5) during insertion of a salty tracer impulse (18.4 fps). The integral mixing time is detected from the logarithmic variance of the reconstructed global average conductivity signal *C* according to

$$\log\sigma^2 = \log(C'-1)^2 \quad (5)$$

where C' is the normalized global average conductivity from

$$C' = \frac{C - C_0}{C_\infty - C_0} \tag{6}$$

and C_0 is the average conductivity level before the tracer injection at t = 7 s and C_∞ is the average at final equilibrium conductivity level (100% mixedness) (Paul et al. 2004). The logarithmic variance allows better resolution of the fine scale around equilibrium and thus a more accurate detection of the 95% mixing time. The latter is reached where the signal falls below $\log\sigma^2$ = -2.602 and C' stays within the ±5% tolerance limits around the equilibrium conductivity level C_∞. The normalized global average conductivity C' and the logarithmic variance for off-bottom clearance C_1 are depicted in Figure 6. The resulting 95% mixing times are t_m = 11.6 s and t_m = 15.6 s for off-bottom clearance C_1 and C_2, respectively.

It is assumed that the temporal evolution of the changes in C' induced by the injection of the salt tracer are adequately described by the exponential expression

$$C' = 1 - \exp\left(-\frac{t_m}{t_c}\right) \tag{7}$$

According to Paul et al. $t_m / t_c \approx 3...5$ can be used as design approximation for mixing vessels with standard geometries (Paul et al. 2004). Although the geometry of the fermenter is different from the standard, especially regarding H/T < 1, a strong correlation is assumed for $t_c \propto t_m$ considering (7). Therefore, the mixing time is used in comparison with the measured circulation times from ERT and sensor particles. In this manner, the increase of the mixing time is also in good agreement with the increase of the estimated circulation time derived from the streamlines of the simulated dispersed phase.

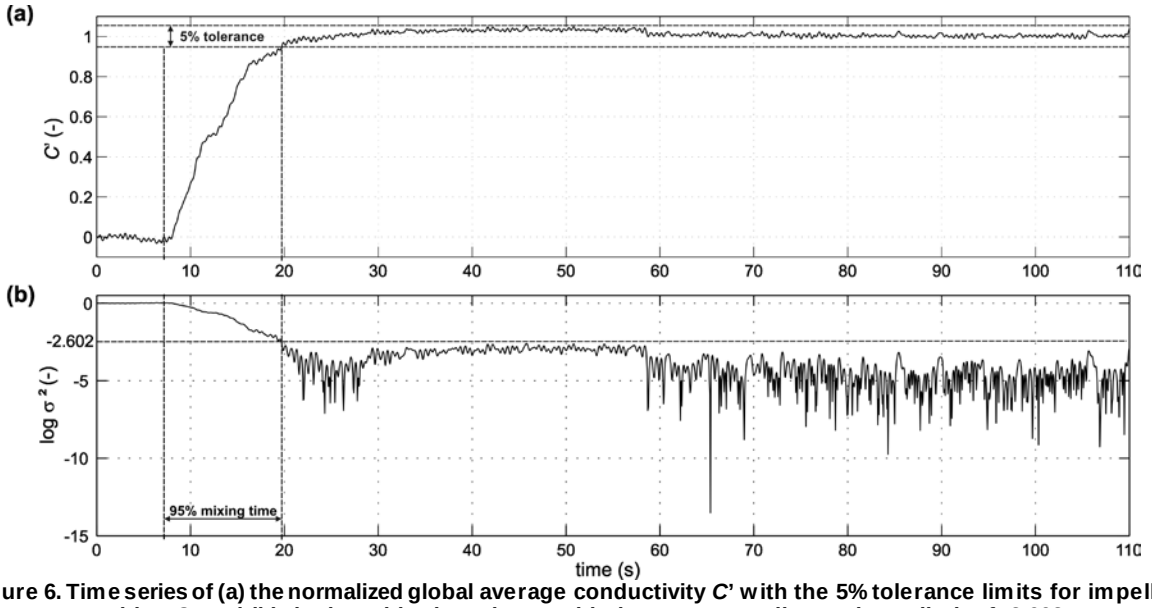

Figure 6. Time series of (a) the normalized global average conductivity C' with the 5% tolerance limits for impeller position C_1 and (b) the logarithmic variance with the corresponding variance limit of -2.602.

3.2.2 Detection and tracking of the sensor particle

Detectability of the sensor particle with the ERT system is due to the high contrast of the non-conducting sensor particle volume and the highly conducting liquid (C = 15 mS/cm). Although the soft-field measurement does not allow accurate reconstruction of the sensor particle volume there is still a significant contrast in the reconstructed images (Figure 7). The sensor particle is giving more than 5% of signal variation at the vessel wall in this ERT configuration, which is comparable to the results of Salem et al. (2001). However, the volume ratio of the vessel and the sensor particle is slightly higher than in the experiment of Salem et al. (2001) with 800 and 1408, respectively. Thus, detectability has to be approved for application of the method to larger vessels.

Improved detection accuracy of the sensor particles centroid of conductivity may be received by application of advanced algorithms for interpolation between the adjacent planes. An enhanced interpolation algorithm is the so called Kriging, which is a linear fill algorithm that has successfully been used for that means by Salem et al. (2001). Moreover, also enhanced reconstruction algorithms may be applied, such as the generalised singular value decomposition (GSVD) algorithm, which utilizes a finite element model of the vessel geometry (Hansen 1989 and 1990). It was successfully used for stirred vessel analysis in several applications by Rodgers et al. (2009 and 2010).

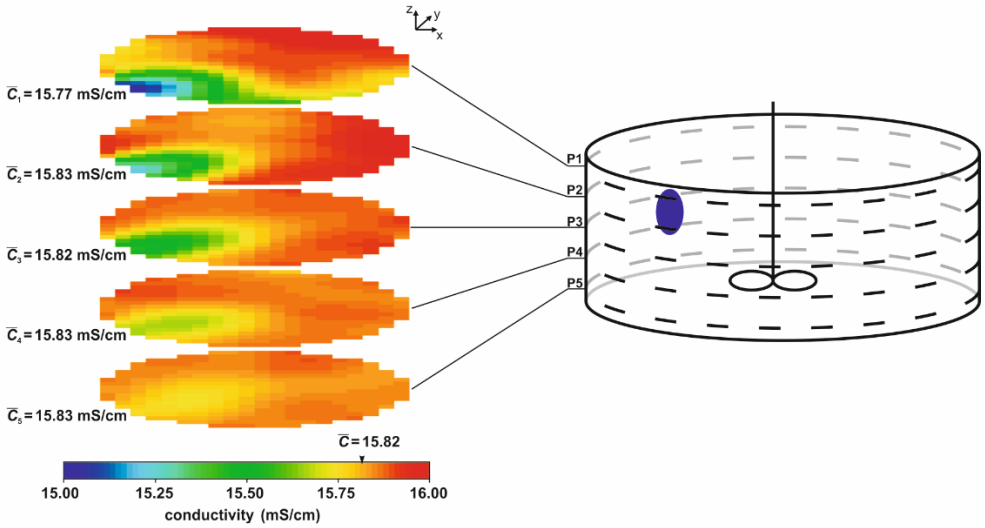

Figure 7. Reconstructed conductivity values at the tomography planes P1…P5 (left) showing the detection strength for the sensor particle at wall position in height of P1 (right).

Application of interpolation algorithms as described by Salem et al. (2001) allows calculation of a finer volume data set from the five reconstructed spatial conductivity distribution planes. The centroid of the sensor particle volume is directly visible around the minimum values of the volume data set. Temporal tracking of the centroid reveals the movement of the sensor particle in the stirred vessel and the long-term trajectory of the center point shows the random flow of the mixing process (Figure 8).

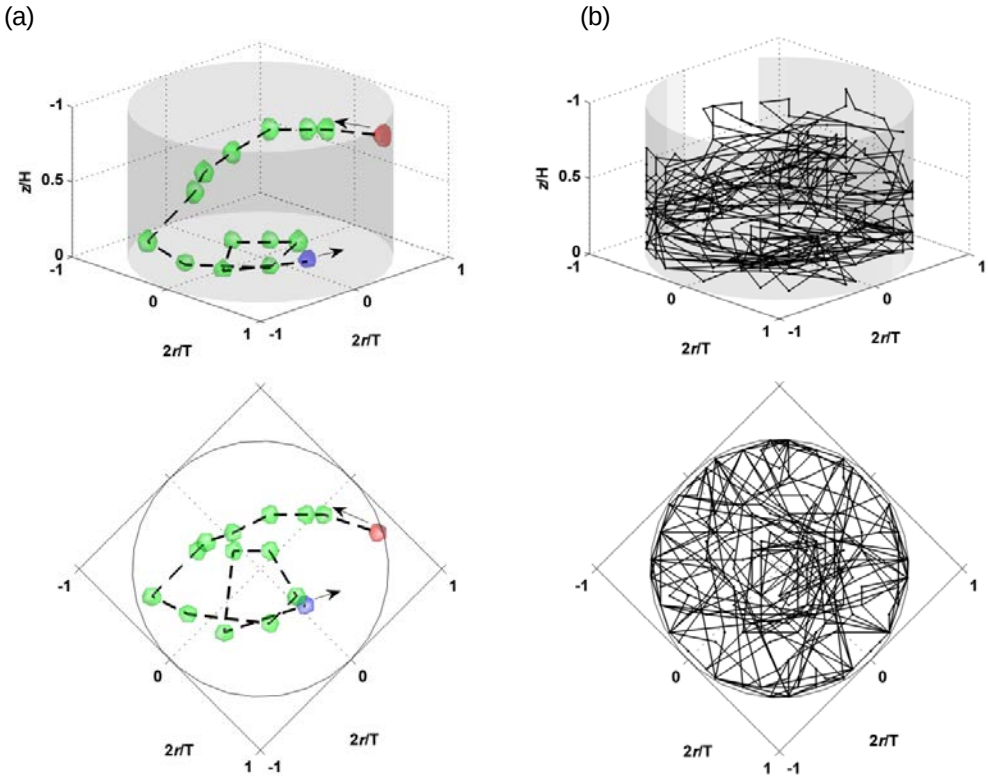

Figure 8. Three dimensional view of (a) centroid movement over a sequence of 5.7 seconds and (b) tracked path of the sensor particle centroid over 190 seconds both from the ERT data.

3.2.3 Sensor particle circulation times

Although five planes are available, the experiments showed that measurement of only two planes (plane P1 and P5) is sufficient to investigate the movement of the sensor particle and particle circulation times in the stirred vessel. This gives an acquisition rate of 18.4 fps. As described earlier the sensor particle is giving a significant contrast in the average conductivity values due to its non-conducting volume in the conducting liquid and thus the movement of the sensor particle is also reflected in the tomography data of the two planes. Especially the maximum conductivity values C_{max} of P1 and P5 reveal the movement of the sensor particle. A sequence of the maximum conductivity of P1 and P5 is depicted in Figure 9 where the passage of the sensor particle is clearly visible from the local minima of the signal for each plane.

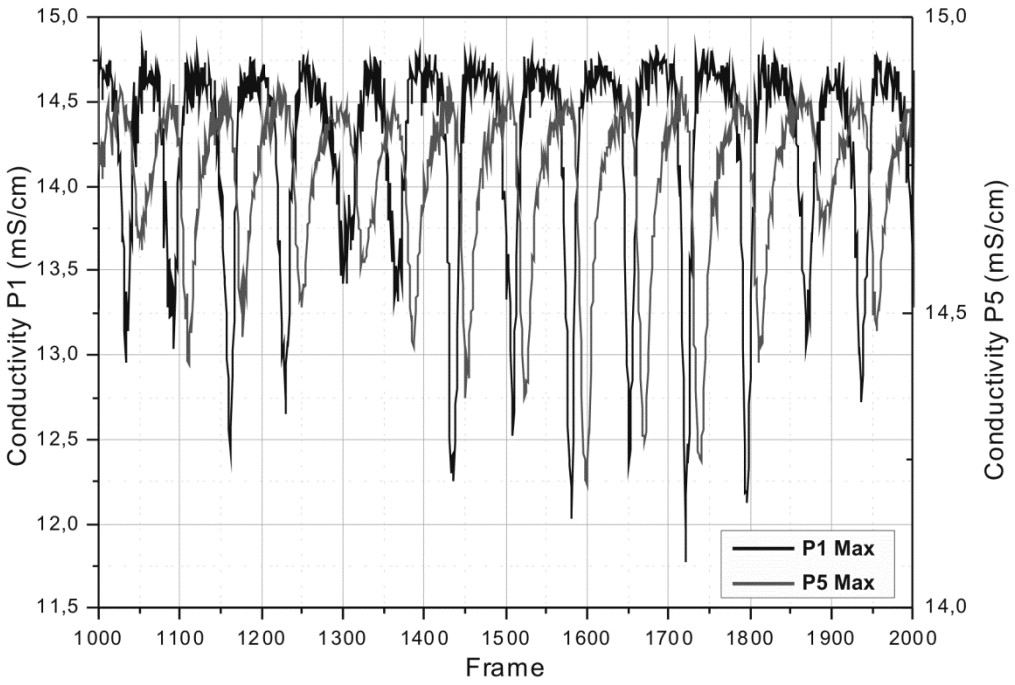

Figure 9. Sequence of the maximum conductivity C_{max} of plane P1 and P5 during the passage of the sensor particle.

Each drop of the fluctuating conductivity signal marks the passage of the sensor particle at the individual tomography plane. According to Barrue et al. the circulation time can be estimated as the time for a fluid element to go again in the circulation loop center plane (Barrue et al., 1999). The circulation loop center plane is between P1 and P5 and therefore also the individual passages of the sensor particle at the plane are contained in the conductivity signal of the ERT. The temporal difference between the consecutive local minima was estimated from the autocorrelation function of the conductivity signal in one plane, i.e. the corresponding lags for the maximum correlation coefficients. The effective circulation time of the sensor particle through the vessel was then calculated from the lags with the acquisition rate of 18.4 fps as listed in Table 1. Only a negligible deviation was observed between the calculated circulation times of P1 and P5. The estimated circulation times of the sensor particle are t_c = 3.8 s and t_c = 4.7 s for off-bottom clearance C_1 and C_2, respectively (Table 1). This increase of the estimated circulation time is confirmed by the increased mixing time measured in the salty tracer ERT experiment.

The uncertainty $u_{tc,ERT}$ of the circulation time can be estimated by the propagation of the given tolerance level u_C of the measured conductivity signal C_{max} with the average derivative $dC_{max}(t)/dt$ of the conductivity at the average conductivity signal at each plane by

$$u_{tc,ERT} = \frac{u_C}{dC_{max}/dt}. \quad (8)$$

The tolerance level u_C is calculated based on the accuracy of the ERT system of ±3% at the average value of C_{max} for each ERT plane. The estimated values of $u_{tc,ERT}$ are 0.62 s and 0.07 s for P_1 and P_2, respectively (Table 1).

Table 1. Estimated circulation times and uncertainties of the sensor particle from the conductivity measurements of the two tomography planes P1 and P5 for off-bottom clearance C_1 and C_2.

		C_1			C_2		
		P1	P5	average	P1	P5	average
lags		69	71		87	85	
t_c	(s)	3.75	3.86	3.80	4.73	4.62	4.67
$/C_{max}$	(mS/cm)	14.75	14.29		15.61	15.07	
$/dC_{max}/dt$	(ms/(cm*s))	0.71	4.14		0.75	6.56	
u_C	(mS/cm)	0.44	0.43		0.47	0.45	
$u_{tc,ERT}$	(s)	0.62	0.10		0.62	0.07	

3.3 Sensor Particle Results

3.3.1 Axial position and axial residence profile of the sensor particle

The axial movement $z(t)$ of the sensor particle in the fluid flow is calculated from the measured immersion depth as function of the ambient hydrostatic pressure $p(t)$ by

$$z(t) = H - \frac{p(t)-p_0}{\rho_f \cdot g}, \quad (9)$$

where p_0 is the atmospheric pressure, ρ_f is the fluid density and g is the gravitational acceleration. In this experiment the axial position of the sensor particle centroid is also available from the processed ERT data and allows validation of the sensor particle measurements. The temporal evolution of the axial coordinate z of the reconstructed trajectory confirms the measured axial position of the sensor particle (Figure 10). This proves the credibility of the immersion depth measurement of the sensor particle for the axial position estimation.

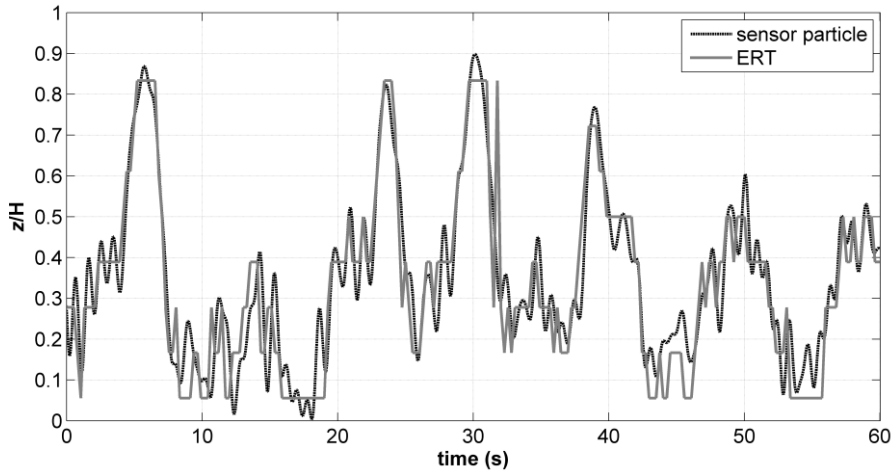

Figure 10. Simultaneously acquired sequence of the axial sensor particle position in the stirred vessel based on the measured ambient pressure by (9) and also the reconstructed sensor particle centroid from ERT data.

Furthermore, the data of $z(t)$ derived from (9) and the ERT data were converted into axial residence profiles by application of statistical analysis methods, namely the discrete probability density function (pdf) of the axial position z. This approach is similar to the probability of presence plots derived by Barrue et al. (1999). The axial residence profiles of the sensor particle centroid measured by the sensor particle and the ERT system are depicted in Figure 11 for both impeller positions. Changes of the mixing conditions induced by the impeller position are clearly visibly from the differences between the residence profiles. The residence profiles at C_2 are distributed more evenly over the height of the vessel than at C_1. This indicates enhanced mixing conditions and an improved axial homogeneity of

the substrates at C_2, which was not observable from the only mixing time experiment. These results confirm the findings in the pilot fermenter where also an improved axial homogeneity was observed for the higher off-bottom clearance of the impeller (Reinecke et al. 2012). The increased characteristic circulation time of the sensor particles indicated longer trajectories and thus that the flow reaches also further ranges of the pilot fermenter vessel compared to the lower off-bottom clearance of the impeller (Reinecke et al. 2012). A probable reason for this effect is the reduced deflection loss in the circulation flow at the vessel bottom for the higher off-bottom clearance of the impeller (Schubert 2003).

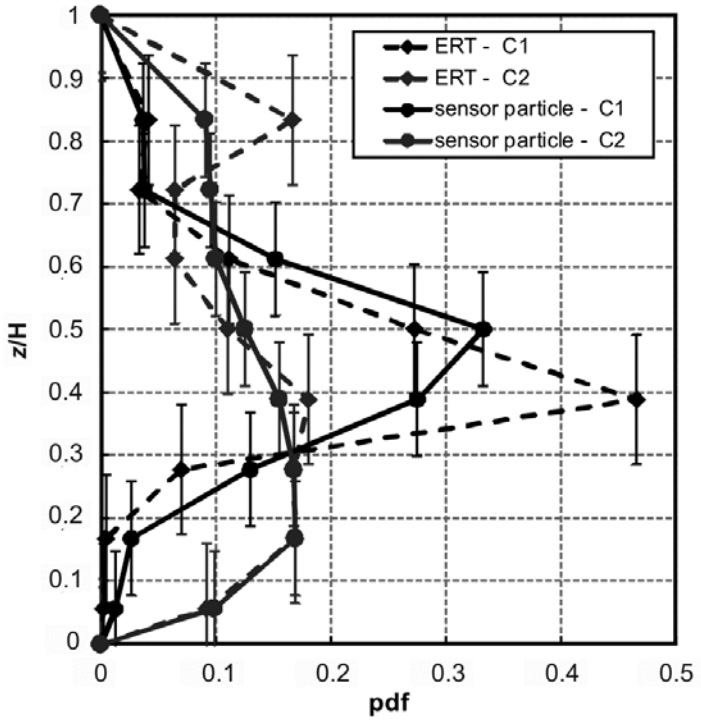

Figure 11. Axial residence profiles with the corresponding uncertainty of the sensor particle centroid measured by the sensor particle and the ERT system.

3.3.2 Estimation of fluid circulation times and distributions

An estimate of the individual fluid circulation time t_c is given by the period between consecutive passages of the sensor particle through the impeller plane in axial downward direction, which is directly extracted from $z(t)$. The circulation time distribution is based on the population of the individual circulation times. This approach was also suggested by Reinecke et al. (2012). The resulting circulation time distributions and the corresponding statistical moments for both impeller positions are depicted in Figure 12. The uncertainty u_{tc} of the circulation time can be estimated by the propagation of the given uncertainty of the measured immersion depth u_z with the derivative $dz(t)/dt$ of the vertical position, i.e. the vertical velocity, during the passage of the impeller plane by

$$u_{\mathrm{tc}} = \frac{u_{\mathrm{z}}}{\mathrm{d}z/\mathrm{d}t}. \qquad (10)$$

The average vertical velocity of the sensor particle during the passage of the impeller plane in axial downward direction is 0.52 $m \cdot s^{-1}$ for C_1 and 0.39 $m \cdot s^{-1}$ for C_2. Thus, according to (10) u_{tc} is $4 \cdot 10^{-2}$ s and $6 \cdot 10^{-2}$ s for C_1 and C_2, respectively.
The expected values of the distributions are estimates of the average liquid circulation times t_c = 3.6 s and t_c = 4.3 s for off-bottom clearance C_1 and C_2, respectively. These values are in agreement with the average circulation times of the sensor particle t_c = 3.8 s and t_c = 4.7 s that were calculated from the ERT measurements. This proves the suitability of the algorithm that is applied to extract the circulation time distributions from the sensor particle data.

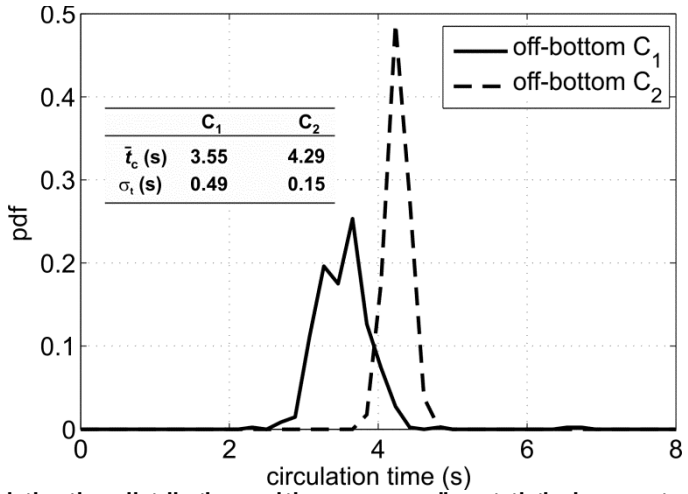

Figure 12. Extracted circulation time distribution and the corresponding statistical parameters from the sensor particle data for off-bottom clearance C_1 und C_2.

In comparison to the simulation results the sensor particle data give an adequate estimate of the average circulation times (Table 2). Especially the relative changes due to the change of the off-bottom clearance of the impeller are reflected properly and confirm the conclusions in the larger pilot fermenter (Reinecke et al., 2012). The increase of the measured mixing time for C_2 is reflected by the values of the circulation time from simulation, ERT and sensor particle comparably. In conclusion, the obtained data of the sensor particle give very good qualitative information. However, there is a significant uncertainty associated with quantitative data due to the scaling of the small vessel geometry and the size of the sensor particle.

Table 2. List of the measured mean circulation times t_c derived from the circulation time distribution (sensor particle) and the conductivity values (ERT + sensor particle) compared to the estimated circulation times from the streamlines of the simulated dispersed phase together with the estimated level of uncertainty.

	t_c(s)		
	C_1	C_2	$u_{tc,max}$(s)
simulation	3.91	4.16	1.0
ERT + sensor particle	3.77	4.68	0.6
sensor particle	3.55	4.29	0.1

4 CONCLUSIONS

An experimental study of the fluid circulation and the macro-mixing process in a stirred model fermenter of non-Newtonian liquid was conducted, where the technique of flow following sensor particles was applied together with an electrical resistance tomography system (ERT). Based on the measured temporal evolution of the axial position of the sensor particle axial residence profiles as well as circulation time distributions and the average circulation times were extracted. The axial residence profiles reveal the impact of the impeller configuration to the axial mixing homogeneity. Furthermore, average circulation times of the sensor particle were calculated from the temporal difference between the drops of the fluctuating conductivity signals from the ERT measurements. Moreover, the liquid mixing times were measured in ERT NaCl tracer experiments and used for validation of the

estimations of ERT and sensor particle. The estimated average circulation times of ERT, sensor particle and simulation are comparable for the two investigated off-bottom clearances in the range of the existing uncertainties. The relative changes due to the axial shift of the impeller position are reflected properly in the estimated circulation times and are in agreement with the findings of the study at the pilot fermenter (Reinecke et al., 2012). It is evident, that a slight increase of the off-bottom clearance of the impeller has a significant positive influence to the axial mixing homogeneity although the detected circulation and mixing times are increased. Only the spatial information of the sensor particles did reveal this hydrodynamic effect. Moreover, the results of the experimental work are supported by numerical simulations of the flow in the fermenter.
These results prove the feasibility of the applied method also for further investigation of the complex flows in biogas fermenters. Future work may encompass further validation also in up-scaled experiments and thus an improved scaling of the experiment. Especially the flow following sensor particles enable the investigation of the mixing process also in reactors where ERT may not be applicable due to the geometries and dimensions of the vessel and the harsh internal conditions. Moreover, improved tomogram interpolation procedures such as Kriging and enhanced reconstruction algorithms such as GSVD will be considered for the ERT data processing.

5 REFERENCES

BARRUE, H., XUEREB, C., PITIOT, P., FALK, L., BERTRAND, J. (1999), Comparison of Experimental and Computational Particle Trajectories in a Stirred Vessel, *Chem. Eng. Technol.*, 22 511-522.

BARNEVELD, J. V., SMIT, W., OOSTERHUIS, N. M. G., PRAGT H. J. (1987), Measuring the liquid circulation time in a large gas-liquid contractor by means of a radio pill. Part 2. Circulation time distribution, Ind. Eng. Chem. Res., 26 2192–2195

BRUENING, S. (2012), Strömungssimulation als Werkzeug zur Bioreaktorcharakterisierung, Dissertation, TU München, 2012.

BRYANT, J. (1969), *Mixing in Fermenters*, Dissertation, University of Cambridge.

BURNETT-THOMPSON, A., YORK, T. A. (2007), A 3D Acoustic Local Positioning System to Track a Neutrally Bouyant Flow Follower. *In IEEE Instrumentation and Measurement Technology Conference (IMTC 2007), Warzaw, Poland*.

DAY, A. (1975), *Mixing in stirred tanks*, Dissertation, University of Exeter.

DENG, Z., CARLSON, T.J., DUNCAN, J.P., RICHMOND, M.C. (2007), Six-Degree-of-Freedom Sensor Fish Design and Instrumentation, *Sensors Journal*, 7 3399-3415.

FANGARY, Y.S., BARIGOU, M., SEVILLE, J.P.K., PARKER, D. J. (2000), Fluid trajectories in a stirred vessel of non-Newtonian liquid using positron emission particle tracking, *Chem. Eng. Sci.*, 55 5969-5979.

HANSEN, P. C. (1989), Regularization, gsvd and truncated gsvd, BIT Numerical Mathematics 29, 491-504.

HANSEN, P. C. (1990), The discrete picard condition for discrete ill-posed problems, BIT Numerical Mathematics 30, 658-672.

LUO, H.-P., AL_DAHHAN, M. H. (2008), Macro-mixing in a draft-tube airlift bioreactor, *Chem. Eng. Sci.*, 63 1572-1585.

MANN, R., DICKIN, F.J., WANG, M., DYAKOWSKI, T., WILLIAMS, R.A., EDWARDS, R.B., FORREST, A.E. and HOLDEN, P.J. (1997), Application of electrical resistance tomography to interrogate mixing processes at plant scale, Chem. Eng. Sci., 52, 2087-2097.

MAVROS, P. (2001), Flow visualization in stirred vessels - a review of experimental techniques, *Trans. ICHemE*, 79 113-127.

MONTANTE, G., PAGLIANTI, A. (2015), Fluid dynamics characterization of a stirred model bio-methanation digester, Chem. Eng. Res. Des., 93, 38–47.

PASCHEDAG, A. (2004), CFD in der Verfahrenstechnik. Allgemeine Grundlagen und mehrphasige Anwendungen, WILEY-YCH Verlag, Weinheim, 2004.

PATTERSON, E.E., HALOW, J., DAW, S. (2010), Innovative Method Using Magnetic Particle Tracking to Measure Solids Circulation in a Spouted Fluidized Bed, *Ind. Eng. Chem. Res.*, 49 5037-5043.

PAUL, E.L., ATIEMO-OBENG, V.A., KRESTA, S.M. (2004), *Handbook of Industrial Mixing Science and Practice*, WILEY-INTERSCIENCE.

POTTINGER, M. G., YORK, T. A. (2011), Modified algorithm for localisation of wireless sensors in confined spaces, *In IEEE Topical Conference on Wireless Sensors and Sensor Networks (WiSNet), Phoenix, USA.*

REINECKE, S., DEUTSCHMANN, A., JOBST, K. KRYK, H., FRIEDRICH, E., HAMPEL, U. (2012), Flow following sensor particles - Validation and macro-mixing analysis in a stirred fermentation vessel with a highly viscous substrate, *Biochem. Eng. J.*, 69 159-171.

REINECKE, S. F. (2014), Instrumentierte Strömungsfolger zur Prozessdiagnose in gerührten Fermentern, Dissertation, Dresdner Beiträge zur Sensorik, Band 52, TUDpress, 2014, ISBN: 978-3-944331-50-8.

RODGERS, T. L., STEPHENSON, D. R., COOKE, M., YORK, T. A., MANN, R. (2009), Tomographic imaging during semi-batch reactive precipitation of barium sulphate in a stirred vessel, Chem. Eng. Res. Des.,87 615-626.

RODGERS, T. L., SIPERSTEIN, F. R., MANN, R., YORK, T. A. KOWALSKI, A. (2011). Comparison of a networks-of-zones fluid mixing model for a baffled stirred vessel with three-dimensional electrical resistance tomography, Meas. Sci. Technol., 22.

SALEM, K., KLING, K., MANN, R. (2001), Application of Electrical Resistance Tomography (ERT) to monitor a flow-follower in a stirred vessel. In 2nd World Congress on Industrial Process Tomography (WCIPT2), Hannover.

SCHUBERT, H. (2003), *Handbuch der Mechanischen Verfahrenstechnik*, WILEY-VCH.

THIELE, S., DA SILVA, M.J., Hampel, U. 2010, Autonomous sensor particle for parameter tracking in large vessels, *Meas. Sci. Technol.*, 21.

WADKE, P.M., HOUNSLOW, M.J. SALMAN, A.D. (2005), The 'SMART' SPHERE Experimental Results, *Chem. Eng. Res. Des.*, 83 1265-1340.

WOLLNY, S. (2010), Experimentelle und numerische Untersuchungen zur Partikelbeanspruchung in gerührten Bio-Reaktoren, Dissertation, TU Berlin, Faculty Process Sciences, 2010.

WU, B. (2011), CFD investigation of turbulence models for mechanical agitation of non-Newtonian fluids in anaerobic digesters, Water Res., 45 2082-2094.

YORK, T. A., GREEN, P.N., GREEN, P.R., HUSSAIN, M., NAWAZ, S., PHASOULIOTIS, A., QU, Z., STANLEY, S., TRIGONI, N., WATSON, S. (2012), Acoustic sensor networks for decommissioning, *Trans. Inst. Meas. & Control*, 45.

ZHANG, Y., YU, G., YU, L., SIDDHU, M. A., GAO, M., ABDELTAWAB, A. A., AL-DEYAB, S. S., CHEN, X. (2016), Computational fluid dynamics study on mixing mode and power consumption in anaerobic mono- and co-digestion, Bioresour. Technol., 203 166-172.